Assessment of discrete Fourier transform as a pre-sizing tool for large-scale energy storage in renewable energy systems

Rafael d'Amore-Domenech[a,], Ernesto Madariaga-González[a], Diego Díaz-Cuenca[a], Vladimir L. Meca[a], Antonio Villalba-Herreros[a], Teresa J. Leo[a]*
[a] *Universidad Politécnica de Madrid, Madrid, Spain*
[*] r.damore@upm.es

Abstract:

The increasing penetration of variable renewable energy sources introduces significant temporal variability in power systems, making energy storage a key design variable. This work assesses the use of the discrete Fourier Transform (DFT) as a tool for the preliminary selection and sizing of energy storage systems in renewable-based isolated energy communities. The proposed approach is based on the spectral decomposition of the residual power signal, defined as the difference between renewable generation and electricity demand, in order to identify dominant temporal scales and associate them with appropriate storage technologies.

A case study representing an isolated energy system in the Madrid (Spain) region is considered, combining photovoltaic and wind generation. The residual signal is analyzed in the frequency domain, and a simplified techno-economic model is applied to determine a transition between battery energy storage systems (BESS) and hydrogen energy storage systems (HESS). The results show the emergence of a characteristic transition period of approximately 70 hours, separating short- and long-duration storage roles.

The DFT-based pre-sizing is compared with time-domain simulations, showing good agreement in terms of order of magnitude for key design variables, particularly in the estimation of long-duration storage requirements and the associated additional renewable installed power needed to compensate for hydrogen conversion losses. In addition, inverse reconstruction of the low-frequency signal shows good agreement with the time-domain simulation of the hydrogen storage operation under a rule-based scenario.

The results suggest that the residual power signal contains sufficient spectral information to support first-order storage design decisions. This method could be used as a complementary front-end tool to guide technology selection and reduce the computational effort required in subsequent optimization stages.

Keywords:

Renewable Energy; Energy Storage; Discrete Fourier Transform.

1. Introduction

The rapid expansion of variable renewable energy sources like solar PV and wind power is transforming energy system planning into a flexibility allocation problem, in which storage is no longer a marginal component but a central design variable. In this context, the key question is not only how much storage should be installed, but also which storage technologies are most suitable for balancing variability across different temporal scales. Storage planning is therefore an intrinsically coupled problem of technology selection and sizing, where power rating, energy storage capacity, efficiency, cycling capability, lifetime and cost must be considered simultaneously [1–3].

This challenge is reinforced by the strong heterogeneity of available storage technologies. Lithium-ion batteries are generally well suited to short-duration, high-efficiency and high-power applications, whereas hydrogen-based storage systems, comprising at least an electrolyzer, a storage stage and a reconversion unit such as a fuel cell or gas turbine, become attractive when very large energy storage capacity and long discharge durations are required, despite their lower round-trip efficiency. As a result, storage technologies do not

compete uniformly over the same operating space; rather, their suitability depends on the time scale, cycling regime and service to be provided. This has motivated a broad literature on storage technology evaluation, ranging from techno-economic optimization to multi-criteria decision-making frameworks tailored to specific grid services and application contexts [1,3,4].

In the literature, the most rigorous way to address storage selection and sizing has traditionally been full chronological optimization based on high-resolution time series of demand, renewable generation and, in some cases, price signals. Deterministic, stochastic and robust formulations have all been proposed, together with increasingly detailed models accounting for degradation, stacked value streams and operational constraints [2]. However, as model fidelity increases, so does computational burden. This is particularly relevant in renewable-dominated systems, where the need to preserve hourly or sub-hourly chronology conflicts with the desire to explore multiple storage candidates, multiple years of data and broad design spaces.

To alleviate this burden, temporal reduction has become one of the dominant strategies in energy system planning. Representative days or weeks selected by clustering algorithms such as k-means, k-medoids or related approaches are now widely used to reduce the dimensionality of the problem while preserving the main statistical features of the underlying time series [5–7]. Yet the literature also shows that temporal reduction is not neutral. The treatment of chronology, ramping behavior, cluster weights and extreme periods can significantly affect both system costs and the selected technology portfolio. Representative-day methods may underestimate storage needs when intraday ramps, interday energy transfers or extreme net-load events are not properly retained [6–9]. These limitations become even more critical for long-duration storage, whose value depends on balancing horizons extending well beyond isolated daily cycles [6,9].

A parallel line of research has explored signal decomposition methods to extract the characteristic time scales of renewable variability and to associate them with different storage functions. In these approaches, the fluctuating signal is decomposed in the frequency or time–frequency domain, and different bands are assigned to storage technologies with complementary dynamic capabilities. Discrete Fourier Transform (DFT) and Discrete Wavelet Transform (DWT) have been applied to wind or renewable output smoothing, as well as to hybrid storage planning problems involving batteries, supercapacitors and, more recently, hydrogen-based storage [10–12]. These studies are important because they recognize an essential physical point: storage is fundamentally a multiscale flexibility resource, and the natural domain for classifying flexibility needs is, at least partly, the temporal-frequency domain.

However, frequency-domain approaches have so far been used mainly to smooth renewable generation profiles or to distribute fluctuations among technologies that were already chosen a priori. Their use as an explicit front-end tool for technology selection and rapid pre-sizing from the residual power signal remains much more limited. From a system-design perspective, the relevant signal is not renewable generation alone, but the residual power profile, i.e., the mismatch between renewable generation and demand. This residual signal directly represents the power that storage must absorb during surplus periods and deliver during deficit periods and therefore provides a more system-relevant basis for identifying whether short-duration electrochemical storage, long-duration hydrogen storage, or a hybrid combination is more appropriate.

Against this background, this work assesses a DFT-based approach applied to the residual power signal as a practical methodology for the selection and preliminary sizing of large-scale energy storage systems. The central hypothesis is not that spectral analysis can replace chronological simulation or full techno-economic optimization, but rather that it can provide a rapid and physically interpretable pre-design layer. By identifying the dominant temporal scales of the residual power profile and associating them with characteristic power and energy requirements, the method can generate informed initial estimates of the storage technologies and capacities most likely to be relevant. These estimates can then be refined through time-domain simulation including conversion efficiencies, operational constraints and extreme events. In this sense, the contribution of the paper is an assessment of the usefulness and limits of DFT as a decision-support tool for storage planning in renewable-dominated systems, particularly for distinguishing the complementary roles of lithium-ion batteries and hydrogen-based storage.

This work is organized as follows. Section 2 describes the methodological framework, including the spectral decomposition of the residual power signal and the modelling of the storage systems. Section 3 presents the main results, including the identification of dominant temporal scales and the assessment of the DFT-based pre-sizing approach against time-domain simulations. Section 4 discusses the main findings and limitations of the methodology, and Section 5 concludes the paper with key insights and directions for future work.

2. Methods

The methodology combines spectral analysis of the residual power signal with time-domain simulation. The residual signal—defined as the difference between renewable generation and electricity demand—is used to identify dominant temporal scales and allocate balancing duties between storage technologies with different operating ranges. In the present work, short- and medium-duration fluctuations are associated with battery storage, whereas long-duration imbalances are assigned to hydrogen-based storage.

The analysis proceeds in three stages. First, the residual power signal is constructed and an ideal lossless storage representation is used to characterize intrinsic balancing requirements. Second, the signal is decomposed using the discrete Fourier transform to identify dominant temporal scales. Third, battery and hydrogen storage systems are simulated in the time domain to evaluate the consistency of the spectral pre-sizing and to assess techno-economic performance. Table 1 summarizes all symbols later discussed in this Section.

Table 1. *Symbols and values used in this study.*

Symbol	Definition	Units	Value
A_k	Amplitude of the k-th harmonic component of the residual power signal	kW	–
c_{BESS}	Specific cost of battery energy storage system	€/kWh	400
c_{EL}	Specific cost of electrolyzer system	€/kW	1000
c_{FC}	Specific cost of fuel cell system	€/kW	2500
c_{HS}	Specific cost of hydrogen storage	€/kWh	0.03
DoD	Depth of discharge of the battery	–	0.7
E_b	Energy exchanged in one half-cycle of an ideal sinusoidal signal	kWh	-
$E_{ideal}(t_n)$	Stored energy in the ideal storage system at time step t_n	kWh	–
f_{Nyq}	Nyquist frequency	h^{-1}	–
k	Harmonic index of the discrete Fourier transform	–	–
$\mathrm{LHV}_{\mathrm{H_2}}$	Lower heating value of hydrogen	kWh/kg	33.333
m_{H_2}	Stored hydrogen mass	kg	–
N	Number of time steps in the analyzed period	–	8784
T_k	Period associated with the k-th harmonic	h	–
Δt	Time step resolution	h	1
$\eta_{ch,B}$	Battery charging efficiency	–	0.95
$\eta_{dis,B}$	Battery discharging efficiency	–	0.95
η_{el}	Electrolyzer efficiency	–	0.63
η_{fc}	Fuel cell efficiency	–	0.5
α_{PV}	Number of photovoltaic panels	–	3615 / 9095
α_{WT}	Number of wind turbines	–	5
$\dot{W}_{dem}(t_n)$	Electrical demand at time step t_n	kW	–
$\dot{W}_{PV}(t_n)$	Electrical power generated by the photovoltaic system	kW	–
$\dot{W}_{WT}(t_n)$	Electrical power generated by the wind system	kW	–
$\dot{W}_{ren}(t_n)$	Total renewable power generation	kW	–
$\dot{W}_{res}(t_n)$	Residual power (generation minus demand)	kW	–
$\widehat{W}_{res,k}$	Fourier coefficient of the residual power signal	kW	–
$\dot{W}_k(t)$	k-th harmonic component of the residual power signal	kW	–

2.1. Time series and residual power signal

The discrete sampling times are defined as

$$t_n = n\Delta t, n = 0,1, \dots, N-1 \quad (1)$$

where $\Delta t = 1\ \mathrm{h}$ is the sampling interval and N is the total number of time steps.

The electrical demand is denoted by $\dot{W}_{\mathrm{dem}}(t_n)$. Renewable generation is provided by a combination of photovoltaic and wind power. The reference generation profiles corresponding to one unit of installed photovoltaic and wind nominal power are denoted by $\dot{W}_{\mathrm{PV},0}(t_n)$and $\dot{W}_{\mathrm{WT},0}(t_n)$, respectively. These profiles are scaled by the number of photovoltaic panels α_{PV} and wind turbines α_{WT}:

$$\dot{W}_{\mathrm{PV}}(t_n) = \alpha_{\mathrm{PV}}\, \dot{W}_{\mathrm{PV},0}(t_n) \tag{2}$$

$$\dot{W}_{\mathrm{WT}}(t_n) = \alpha_{\mathrm{WT}}\, \dot{W}_{\mathrm{WT},0}(t_n) \tag{3}$$

The total renewable power generation in the time-domain is therefore

$$\dot{W}_{\mathrm{ren}}(t_n) = \dot{W}_{\mathrm{PV}}(t_n) + \dot{W}_{\mathrm{WT}}(t_n) \tag{4}$$

The residual power signal is defined as

$$\dot{W}_{\mathrm{res}}(t_n) = \dot{W}_{\mathrm{ren}}(t_n) - \dot{W}_{\mathrm{dem}}(t_n) \tag{5}$$

Positive values of $\dot{W}_{\mathrm{res}}$indicate renewable surplus, whereas negative values indicate power deficit. Accordingly, $\dot{W}_{\mathrm{res}}$ represents the net power that must be absorbed or delivered by the storage system.

2.2. Ideal storage representation

To characterize the intrinsic balancing requirement independently of storage technology, an ideal lossless storage system is first considered. Its stored energy evolves according to

$$E_{\mathrm{ideal}}(t_{n+1}) = E_{\mathrm{ideal}}(t_n) + \dot{W}_{\mathrm{res}}(t_n)\Delta t \tag{6}$$

with an arbitrary initial condition, here taken as

$$E_{\mathrm{ideal}}(t_0) = 0 \tag{7}$$

The required ideal storage capacity is estimated from the excursion of this cumulative energy trajectory:

$$E_{\mathrm{cap,ideal}} = \max_n \left(E_{\mathrm{ideal}}(t_n)\right) - \min_n \left(E_{\mathrm{ideal}}(t_n)\right) \tag{8}$$

2.3. Spectral decomposition of the residual power signal

To characterize the temporal structure of the residual power signal, a discrete Fourier Transform (DFT) is applied. The residual power signal $\dot{W}_{\mathrm{res}}(t_n)$, defined at discrete time instants $t_n = n\Delta t$, is transformed into the frequency domain as

$$\widehat{W}_{\mathrm{res},k} = \frac{1}{N}\sum_{n=0}^{N-1} \dot{W}_{\mathrm{res}}\,(t_n)\exp(-j\frac{2\pi kn}{N})\ , \qquad k = 0,1,\dots,N-1 \tag{9}$$

Where N is the total number of samples, and $j = \sqrt{-1}$. The normalization factor $1/N$ ensures that the Fourier coefficients retain the physical units of power and are directly comparable to the original signal.

The discrete frequencies associated with the spectral components are

$$f_k = \frac{k}{N\Delta t} \tag{10}$$

For $k \neq 0$, the characteristic period of the k-th component is

$$T_k = \frac{1}{f_k} \tag{11}$$

The $k = 0$ component corresponds to the mean value of the residual signal and therefore does not define a finite period. This component represents the systematic net annual imbalance between renewable generation and demand. If the resulting value of $\widehat{W}_{\mathrm{res},k=0} \neq 0$, this imbalance must be resolved through renewable capacity tuning or other practices, such as curtailment, or unserved load.

For real-valued signals, such as the residual power signal considered in this work, the Fourier spectrum is Hermitian symmetric, i.e.,

$$\widehat{W}_{\mathrm{res},k} = \widehat{W}^{*}_{\mathrm{res},N-k} \tag{12}$$

which implies that each frequency component at f_k has a corresponding conjugate component at $-f_k$. As a result, each sinusoidal contribution to the signal is represented by a pair of symmetric spectral components. The actual amplitude A_k is thus obtained as

$$A_k = 2\ |\ \widehat{W}_{\mathrm{res},k}\ | \qquad 0 < k < \frac{N}{2} \tag{13}$$

In practice, due to this symmetry, only the range $0 \leq k \leq N/2$ needs to be considered, as it contains all independent spectral information. This one-sided spectrum is used in the present work to identify the dominant

temporal scales of the residual power signal and to relate them to the characteristic operating ranges of different storage technologies.

The magnitude of the Fourier coefficients provides information on the contribution of each temporal scale to the overall balancing problem. The minimum temporal scale that can be represented is limited by the sampling interval. Since the present analysis uses hourly data, sub-hourly fluctuations are not captured.

2.4. Spectral separation into battery and hydrogen bands

The purpose of this step is to define a systematic procedure for assigning different temporal scales of the residual power signal to storage technologies with different characteristic operating ranges. In the present work, this separation is established through a simplified techno-economic comparison between battery energy storage systems (BESS) and hydrogen energy storage systems (HESS), using the spectral information obtained from the discrete Fourier transform.

For an individual harmonic component k, characterized by amplitude A_k and period T_k, an idealized sinusoidal residual power signal is defined as

$$\dot{W}_k(t) = A_k \cos\left(\frac{2\pi}{T_k} t\right) \tag{14}$$

This sinusoidal representation is used as a reference oscillation to evaluate the storage time-domain function associated with a given temporal scale.

For each pair (A_k, T_k), a simplified techno-economic model is applied to estimate the levelized cost of electricity storage for BESS and HESS. The comparison is performed over a prescribed project lifetime L, taken here as 20 years. Degradation effects are neglected at this stage, so the comparison is based on nominal operation.

The result of this harmonic-level comparison is a technology preference as a function of estimated levelized cost of energy storage (LCOES). In this way, the Fourier spectrum can be interpreted not only in terms of temporal scales, but also in terms of the storage technology that is more likely to be economically suitable for balancing fluctuations in each region of the spectrum. When the discrete spectrum exhibits clearly identifiable peaks, the techno-economic comparison can be applied directly to those dominant harmonics. However, in many practical cases the DFT spectrum is noisy and densely populated, which makes the direct interpretation of individual harmonics difficult. In such cases, adjacent harmonics are grouped into logarithmically spaced period bands in order to smooth the spectrum and facilitate interpretation.

Let $T_{\min} = 2\Delta t$ be the minimum resolvable period associated with the Nyquist limit, and let $T_{\max} = N\Delta t$ be the maximum period associated with the full signal duration. The interval $[T_{\min}, T_{\max}]$ is divided into N_b logarithmically spaced bands, such that the ratio r between the upper and lower bounds of consecutive bands is constant:

$$r = \left(\frac{T_{\max}}{T_{\min}}\right)^{1/N_b} \tag{15}$$

If T_b^L and T_b^U denote the lower and upper bounds of band b, then

$$T_b^U = r\, T_b^L \tag{16}$$

with $b = 1,2,\dots,N_b$. In the present work, $N_b = 20$ is adopted as a practical compromise between spectral resolution and robustness of interpretation. The representative period of each band is taken as the geometric mean of its bounds,

$$T_b^* = \sqrt{T_b^L T_b^U} \tag{17}$$

which is consistent with the logarithmic spacing.

To characterize the spectral intensity of each band, an approximation of the equivalent band amplitude is defined from the harmonic amplitudes contained within the interval:

$$A_b^* = \sqrt{\sum_{k \in b} A_k^2} \tag{18}$$

where the summation extends over all harmonics whose characteristic periods satisfy $T_b^L \le T_k < T_b^U$. This root-sum-square definition avoids the artificial overestimation that would arise from direct linear summation of amplitudes while providing a more consistent aggregate indicator of fluctuation intensity within each band.

A representative approximated sinusoidal signal can then be associated with each band as

$$\dot{W}_b(t) = A_b^* \cos\left(\frac{2\pi}{T_b^*}t\right) \tag{19}$$

and the same simplified techno-economic comparison between BESS and HESS can be performed for each band. In this way, the grouped spectrum provides a smoothed map of technology preference across the temporal domain.

2.5. Preliminary sizing of the battery energy storage system

Based on the spectral separation defined in Section 2.4, the short duration components of the residual power signal are associated with battery energy storage. In this step, a preliminary estimation of the required battery energy capacity is obtained using the equivalent sinusoidal representation of each spectral band.

For a given band b, characterized by an approximation of the equivalent amplitude A_b^* and representative period T_b^*, the residual power is approximated with Eq (19). The energy exchanged during a half-cycle (charging or discharging phase) is then estimated by integrating the positive portion of the sinusoidal signal:

$$E_b = \int_0^{T_b^*/2} A_b^* \cos\left(\frac{2\pi}{T_b^*}t\right) dt = \frac{A_b^* T_b^*}{\pi} \tag{20}$$

This quantity represents the characteristic energy swing associated with the fluctuation at that temporal scale. To translate this energy swing into a required battery capacity, a depth of discharge (DoD) constraint is introduced. In the present work, a depth of discharge $\mathrm{DoD} = 0.7$ is assumed, corresponding to operation between 20% and 90% state of charge. The required battery energy capacity for each band is therefore estimated as

$$E_{\mathrm{bat},b} = \frac{E_b}{\mathrm{DoD}} \tag{21}$$

The preliminary battery sizing is obtained by evaluating $E_{\mathrm{bat},b}$ over all spectral bands assigned to battery operation and selecting the maximum value:

$$E_{\mathrm{bat}} = \max_b \left(E_{\mathrm{bat},b}\right) \tag{22}$$

2.6. Battery storage model

The battery storage system is characterized by a charging efficiency $\eta_{\mathrm{ch,B}}$ and a discharging efficiency $\eta_{\mathrm{dis,B}}$. Its stored energy evolves as

$$E_{\mathrm{B}}(t_{n+1}) = E_{\mathrm{B}}(t_n) + \eta_{\mathrm{ch,B}}\dot{W}_{\mathrm{ch,B}}(t_n)\Delta t - \frac{\dot{W}_{\mathrm{dis,B}}(t_n)\Delta t}{\eta_{\mathrm{dis,B}}} \tag{23}$$

subject to

$$0 \le E_{\mathrm{B}}(t_n) \le E_{\mathrm{B,max}} \tag{24}$$
$$0 \le \dot{W}_{\mathrm{ch,B}}(t_n) \le \dot{W}_{\mathrm{ch,B,max}} \tag{25}$$
$$0 \le \dot{W}_{\mathrm{dis,B}}(t_n) \le \dot{W}_{\mathrm{dis,B,max}} \tag{26}$$

the present battery model is intended for methodological assessment rather than for detailed operational optimization. More advanced representations, including power-dependent efficiency, degradation, and thermal effects, should be considered in subsequent stages of analysis once the storage configuration has been identified.

2.7. Hydrogen storage model

The hydrogen storage system consists of an electrolyzer, a hydrogen storage stage, and a reconversion unit, here represented generically as a fuel cell. For notation consistency, the hydrogen inventory is conveniently expressed in terms of stored hydrogen mass $m_{\mathrm{H_2}}(t_n)$. Its evolution is given by

$$m_{\mathrm{H_2}}(t_{n+1}) = m_{\mathrm{H_2}}(t_n) + \frac{\eta_{\mathrm{el}}\dot{W}_{\mathrm{el}}(t_n)\Delta t}{LHV_{\mathrm{H_2}}} - \frac{\dot{W}_{\mathrm{fc}}(t_n)\Delta t}{\eta_{\mathrm{fc}}\mathrm{LHV}_{\mathrm{H_2}}} \tag{27}$$

where η_{el} is the electrolyzer efficiency, $\eta_{\mathrm{fc}}$is the fuel-cell efficiency, and $\mathrm{LHV}_{\mathrm{H_2}}$is the lower heating value of hydrogen. The hydrogen system is subject to

$$0 \le \dot{W}_{\mathrm{el}}(t_n) \le \dot{W}_{\mathrm{el,max}} \tag{28}$$
$$0 \le \dot{W}_{\mathrm{fc}}(t_n) \le \dot{W}_{\mathrm{fc,max}} \tag{29}$$

For comparison with battery storage, it is convenient to express the hydrogen inventory in terms of stored chemical energy:

$$E_{H_2}(t_n) = m_{H_2}(t_n)\,\mathrm{LHV}_{H_2} \tag{30}$$

Substituting into Eq. (27), the system dynamics can equivalently be written in energy form as

$$E_{H_2}(t_{n+1}) = E_{H_2}(t_n) + \eta_{el}\,\dot{W}_{el}(t_n)\,\Delta t - \frac{\dot{W}_{fc}(t_n)\,\Delta t}{\eta_{fc}} \tag{31}$$

which highlights the analogy with the battery storage model, with the key difference that energy conversion occurs through distinct charge (electrolyzer) and discharge (fuel cell) processes with separate efficiencies.

It should be noted that E_{H_2} represents stored chemical energy based on the lower heating value, and not directly usable electrical energy. The effective round-trip efficiency of the hydrogen storage system is therefore governed by the combined performance of the electrolyzer and the reconversion unit.

2.8. Renewable generation scaling to compensate hydrogen storage losses

The use of hydrogen-based storage introduces significant energy losses due to the combined inefficiencies of the electrolyzer and the reconversion unit. As a result, the harmonics corresponding to long periods of the residual power signal, since they are assigned to hydrogen storage, require additional renewable generation in order to compensate for the losses and ensure annual energy balance.

In the present work, all spectral components with characteristic periods above the battery–hydrogen transition threshold are assumed to be processed through the hydrogen storage system. For these components, the effective round-trip efficiency is given by the product $\eta_{el}\eta_{fc}$, and therefore a fraction of the energy is irreversibly lost during each cycle.

To estimate the additional renewable capacity required to compensate for these losses, the long-duration spectral content is represented by an equivalent aggregated sinusoidal component. The equivalent amplitude A^*_{HESS} is obtained using a root-sum-square aggregation of the amplitudes of all harmonics belonging to the hydrogen-dominated spectral range as defined by Eq. (18). For a sinusoidal fluctuation of amplitude A^*_{HESS}, the energy processed during a half-cycle is given by Eq. (20).

Due to the finite round-trip efficiency of the hydrogen storage system $\eta_{el}\eta_{fc}$, only a fraction of this energy can be recovered. The remaining fraction must therefore be compensated for by additional renewable generation.

In the present case study, wind capacity expansion is constrained spatially (max 5 wind turbines), and therefore the additional generation is assumed to be provided exclusively by photovoltaic systems which would allow installing up to 9700 PV panels. Assuming that this additional generation is provided by photovoltaic capacity, the required increase in renewable power can be approximated as

$$\Delta\dot{W}_{PV} \approx (1 - \eta_{el}\eta_{fc})\,A^*_{\mathrm{HESS}} \tag{32}$$

A more detailed assessment is performed in the time-domain simulations.

2.9. Energy management strategy for hybrid BESS–HESS operation

The hybrid storage system is operated using a rule-based energy management strategy that allocates the residual power between battery and hydrogen storage at each time step, prioritizing higher-efficiency technologies.

The battery operates within a constrained state-of-charge range (20–90% of nominal capacity). Under surplus conditions, excess renewable power is first used to charge the battery within its operational limits, and any remaining energy is diverted to hydrogen production. Under deficit conditions, the battery is discharged first, and any remaining demand is supplied by the hydrogen system.

This sequential dispatch reflects the higher round-trip efficiency of batteries, with hydrogen storage acting as a secondary resource for larger imbalances. Hydrogen storage is assumed to be effectively unconstrained in terms of energy storage capacity, consistent with large-scale geological storage.

The strategy does not aim at optimal dispatch, but rather provides a consistent and physically interpretable framework to evaluate the DFT-based pre-sizing methodology. More advanced control strategies could improve performance and are left for future work.

2.10. Spectral reconstruction of the hydrogen-dominated signal using the Inverse Discrete Fourier Transform (IDFT)

To assess the representativeness of the DFT-based spectral decomposition, a partial reconstruction of the residual power signal is performed using the Inverse Discrete Fourier Transform (IDFT).

The reconstruction is restricted to the subset of spectral components assigned to hydrogen storage, i.e., those with characteristic periods above the battery–hydrogen transition threshold defined in Section 2.4. Let $\mathcal{K}_H$ denote the set of indices corresponding to these long-duration components. Using the amplitude–phase representation of the Fourier coefficients, the reconstructed signal is expressed as

$$\dot{W}_{res}^{(H_2)}(t_n) \approx \sum_{k \in \mathcal{K}_H} A_k \cos\left(\frac{2\pi kn}{N} + \phi_k\right) \tag{33}$$

where A_k and ϕ_k are the amplitude and phase of the k-th spectral component, respectively.

The partial reconstruction represents a band-limited version of the residual power signal, retaining only low-frequency components associated with long-term imbalances. It thus provides a spectral approximation of the power ideally assigned to hydrogen storage.

This reconstructed signal is used solely as a reference to compare with the time-domain dispatch from the rule-based strategy. The comparison assesses how well spectral decomposition captures actual storage behavior and highlights its potential for guiding storage allocation in hybrid systems with multiple time scales. The IDFT-based approach can therefore serve as a first-order estimate of storage-specific power profiles, to be refined through time-domain simulation.

2.11. Electricity served and techno-economic indicator

A corresponding levelized cost metric may then be defined for the electricity effectively supplied to the user:

$$LCOE_{\text{served}} = \frac{\sum_{y=0}^{N_y} \frac{C_y}{(1+r)^y}}{\sum_{y=1}^{N_y} \frac{E_{\text{served},y}}{(1+r)^y}} \tag{34}$$

Where C_y represents each cost item in the year y, r stands for the discount rate, and $E_{\text{served},y}$ represents the served energy to the end-user on the year y.

3. Results & Discussion

Figure 1 shows the residual power signal and its spectral representation. The time series (Fig. 1(a)) exhibits strong variability across a wide range of time scales, indicating that the balancing requirement is inherently multiscale. The corresponding DFT spectrum (Fig. 1(b)), expressed in terms of characteristic period T_k, is densely populated at short periods and progressively sparser at longer periods, where higher-amplitude components emerge. However, the discrete spectrum is noisy, particularly at high frequencies, which limits its direct interpretability. To improve clarity, adjacent harmonics are grouped into logarithmically spaced period bands (Section 2.4). This aggregation reduces noise while preserving the overall spectral structure, enabling a clearer distinction between short-duration fluctuations and long-duration components.

These results support the use of spectral decomposition as a basis for separating storage duties across temporal scales.

Figure 2 presents the aggregated spectrum in logarithmically spaced period bands, as defined in Section 2.4. The smoothing procedure reveals a structured distribution of spectral amplitude across temporal scales, enabling the identification of dominant regions that are not apparent in the discrete spectrum. Several characteristic regimes can be observed. Short-duration components (below ~10 h) exhibit relatively low amplitudes, despite their high density in the original spectrum. In contrast, intermediate and long-duration components show significantly higher amplitudes, indicating that a substantial fraction of the balancing requirement is associated with slower fluctuations. In particular, a broad maximum is observed in the range from approximately one day to several days, followed by a gradual decay toward longer periods, with

secondary contributions at seasonal scales. This distribution suggests that different temporal ranges are associated with fundamentally different roles in the balancing problem.

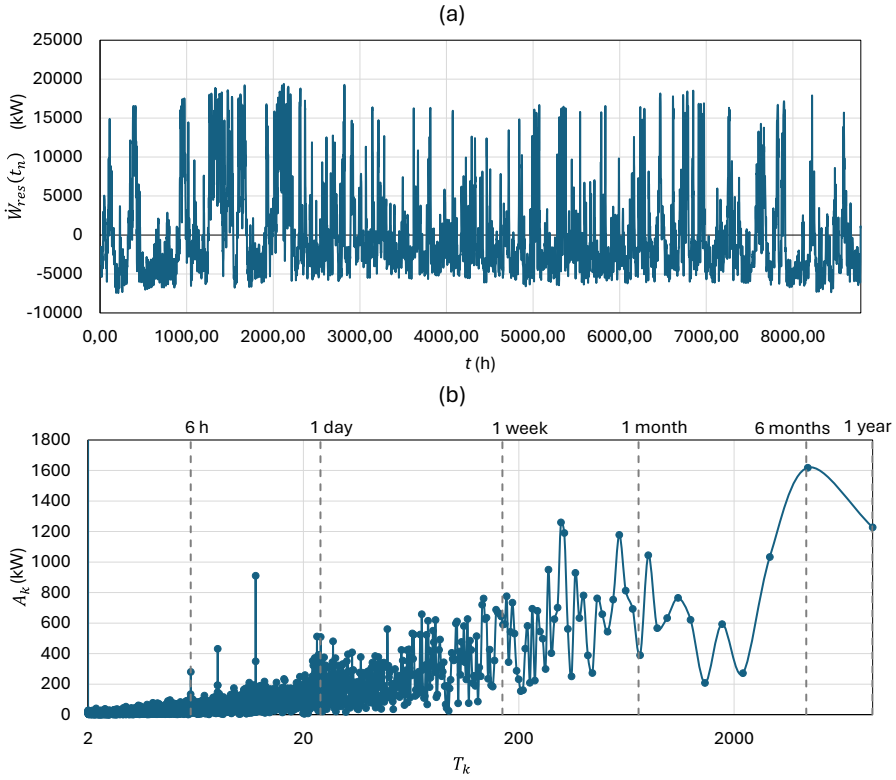

Figure 1. *(a) Residual power signal over one year with hourly resolution. (b) One-sided DFT spectrum expressed in terms of characteristic period T_k, highlighting the multiscale structure of the signal and the increasing dispersion at short periods.*

These results confirm that the residual signal is not spectrally uniform but instead dominated by specific temporal scales. This provides a quantitative basis for defining a transition between storage technologies operating over short and long durations, which is explored in the following section.

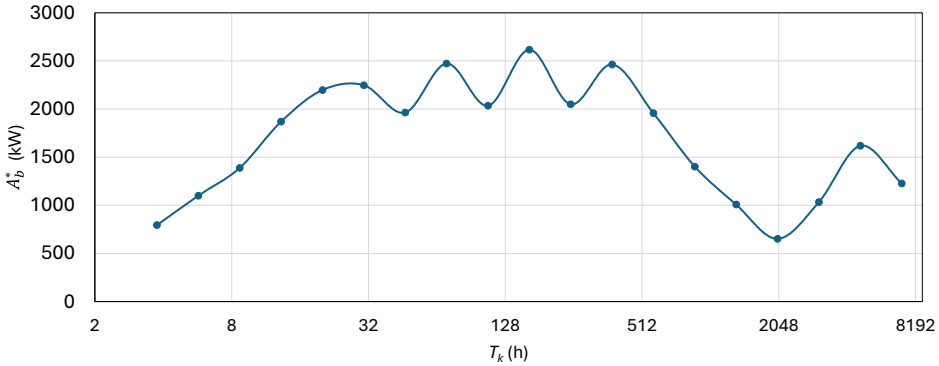

Figure 2. *Aggregated spectral amplitude as a function of characteristic period T_k, obtained using logarithmic band grouping, see Section 2.4. The smoothing reveals dominant temporal scales and highlights the increasing contribution of intermediate and long-duration fluctuations to the overall balancing requirement.*

Figure 3 shows the LCOES for battery (BESS) and hydrogen-based (HESS) systems as a function of the characteristic period T_k, evaluated using the equivalent sinusoidal representation defined in Section 2.4, considering an electricity cost of 50 €/MWh, characteristic of PV contexts. The results reveal two distinct regimes. At short and intermediate periods, BESS exhibits significantly lower storage costs due to its high round-trip efficiency, despite its higher specific investment cost. However, the cost of BESS increases rapidly with increasing period, reflecting the growing energy capacity requirement associated with longer-duration fluctuations. In contrast, the LCOES of HESS remains approximately constant across the entire range of periods. This behavior is driven by the dominance of conversion efficiency losses over energy capacity costs, given the relatively low cost of hydrogen storage per unit of energy. As a result, a transition point emerges at approximately $T \approx 70$h, beyond which hydrogen storage becomes more cost-effective than battery storage.

This transition is not imposed a priori but arises naturally from the interaction between the temporal scale of the fluctuation and the techno-economic characteristics of each technology.

This result provides a physically and economically grounded criterion for separating storage duties between BESS and HESS. Fluctuations with characteristic periods below the transition threshold are more efficiently handled by batteries, while longer-duration components are better suited to hydrogen-based storage.

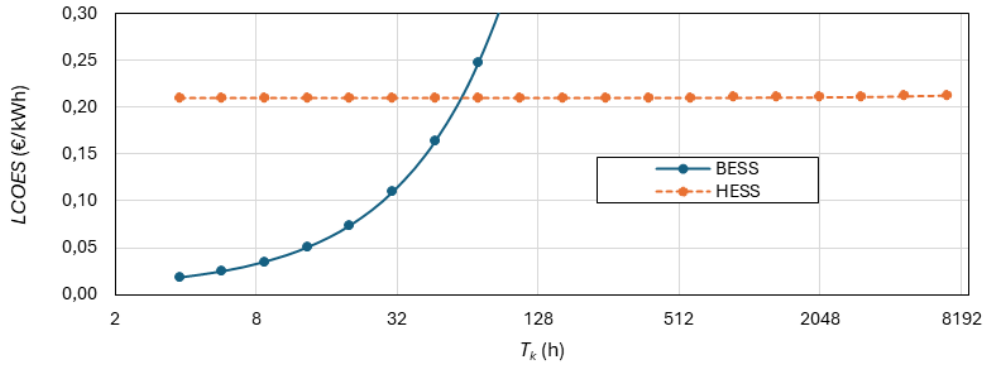

Figure 3. Levelized cost of electricity storage (LCOES) for battery (BESS) and hydrogen storage (HESS) as a function of characteristic period T_k, for an electricity cost of 50 €/MWh (13,89 €/GJ). A transition occurs at approximately 70 h, marking the shift from battery-dominated to hydrogen-dominated storage regimes.

The accuracy of the DFT-based pre-sizing approach is assessed by comparing its predictions with results obtained from time-domain simulations. At the current stage of the analysis, a partial validation is available.

The battery capacity estimated through the DFT-based methodology provides a first-order sizing based on the most demanding spectral component within the battery-dominated range. This value reflects the characteristic energy requirement associated with the dominant short- and medium-duration fluctuations. A full validation of this estimate against optimized time-domain simulations is currently under development and will be included in future work.

A direct comparison is already available for the renewable capacity adjustment required to compensate hydrogen storage inefficiencies. The DFT-based approach predicts an additional photovoltaic capacity of approximately 4092 kW, derived from the aggregated long-duration spectral content (with all the harmonics above the transition threshold $T > 70$ h) and the estimated round-trip losses of the hydrogen system. Time-domain simulations yield a corresponding requirement of approximately 3670 kW, showing good agreement in terms of order of magnitude and overall trend. The relative deviation between both approaches remains limited, indicating that the DFT-based formulation captures the dominant contribution of hydrogen-related losses to the system energy balance. These results suggest that the DFT-based methodology could provide a consistent approximation of the system-level energy requirements associated with long-duration storage, even when simplified assumptions are adopted. It demonstrates that spectral aggregation can be effectively used to estimate the additional renewable capacity required to offset conversion losses.

The present results already indicate that the DFT-based approach could reproduce the main techno-economic drivers governing storage system design.

Figure 4 compares the hydrogen storage power obtained from the time-domain simulation with the reconstructed signal using the IDFT-based spectral filtering approach. The simulated hydrogen power profile (Fig. 4(a)) reflects the actual operation of the system under the rule-based dispatch strategy, including state-of-charge constraints and sequential interactions with the battery system. In contrast, the reconstructed signal (Fig. 4(b)) is obtained by retaining only the spectral components with characteristic periods above the transition threshold ($T > 70$ h), as described in Section 2.10. Despite the simplified nature of the reconstruction, both signals exhibit a similar temporal structure at long time scales. In particular, the IDFT-based signal captures the main low-frequency trends and the general envelope of the hydrogen power profile, indicating that the spectral decomposition successfully isolates the long-duration component of the residual signal. However, notable differences are observed. The reconstructed signal is smoother and lacks the sharp peaks present in the simulated profile, as it does not account for short-term variability or operational constraints. In addition, the simulated signal reflects interactions between storage systems and limitations imposed by the battery state of charge, which are not captured in the purely spectral reconstruction. This disagreement appears to mostly affect the positive band maximums were the rule-based dispatch Fig 4 (a) exhibits higher peaks than the IDFT counterpart (Fig 4 (b)). In practice, this would mean an electrolyzer of about 25% higher rated power than the IDFT prediction, but a fuel cell of about 15% lower rated power than the IDFT prediction.

These results indicate that the IDFT-based approach provides a meaningful approximation of the long-duration storage signal, capturing its dominant temporal structure while neglecting higher-frequency fluctuations and system constraints. This supports the use of spectral filtering as a first-order tool for identifying storage duties, particularly in systems involving multiple storage technologies operating at different time scales.

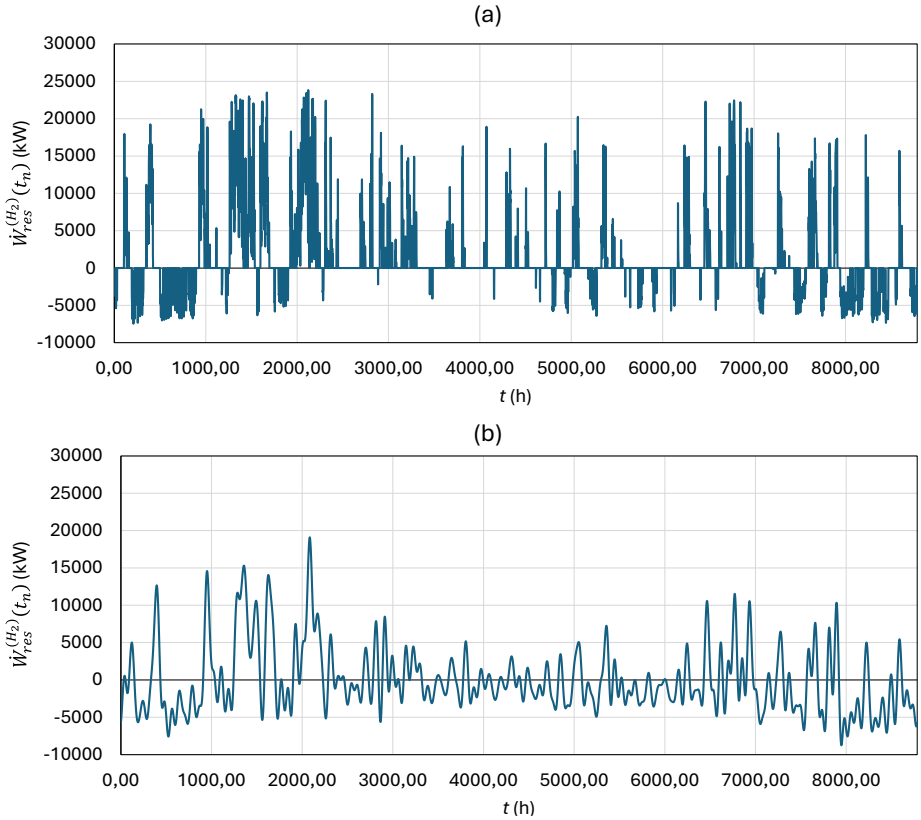

Figure 4. *Comparison between hydrogen storage power obtained from time-domain simulation (a) and IDFT-based reconstruction using only long-duration spectral components ($T > 70$ h) (b). The reconstructed signal captures the low-frequency structure of the hydrogen operation while smoothing short-term variability.*

The results suggest that the DFT-based methodology captures key aspects of the multiscale structure of the residual power signal and its relevance for storage design. Spectral decomposition enables the identification of dominant temporal regimes and their association with specific storage technologies. The observed techno-economic transition between battery and hydrogen storage, together with the reasonable estimation of renewable overcapacity, indicates that the main system-level drivers are captured with acceptable accuracy. However, important limitations remain. The spectral formulation does not account for the chronological and constrained nature of storage operation, such as SOC limits, power constraints, and interdependencies between technologies. As a result, while the IDFT-based reconstruction reproduces the general structure of the signal, it does not capture its detailed temporal dynamics. The results are also sensitive to modelling choices. Band aggregation, spectral metrics, and simplifying assumptions (e.g., constant efficiencies or sinusoidal representation) introduce trade-offs between interpretability and accuracy. Within these constraints, the approach shows potential as a preliminary design tool. It provides a physically interpretable framework to relate temporal variability to storage requirements, supporting first-order design decisions and the identification of dominant time scales. Accordingly, the methodology is better understood as a complementary front-end to time-domain simulation rather than a substitute. Its main value lies in structuring the problem and narrowing the design space prior to more detailed optimization. Further work is required to assess its robustness under different conditions, including comparisons with fully optimized time-domain models, extension to more complex systems, and the use of higher-resolution data and more detailed operational representations.

4. Conclusions

This work presents a Direct Fourier Transform (DFT)-based methodology for the preliminary selection and sizing of energy storage in renewable-based isolated systems. By analyzing the residual power signal in the frequency domain, the approach identifies dominant temporal scales and relates them to storage technologies with different operational characteristics. The results indicate a clear multiscale structure, enabling the identification of a techno-economic transition between battery and hydrogen storage, occurring at around 70 hours in the case study. The method provides estimates consistent in order of magnitude with time-domain simulations, particularly for long-duration storage and renewable overcapacity. The Inverse Direct Fourier

Transform (IDFT) reconstruction further captures the main low-frequency behavior associated with hydrogen storage. The methodology should therefore be interpreted as a physically informed pre-design tool rather than as a replacement for detailed chronological simulation. Its value lies in reducing the design space and supporting an initial allocation of balancing duties between technologies, while reducing the scope of subsequent optimization. Although a fixed cut-off period is used in this work, the same framework could be extended towards more flexible rule-based strategies. For instance, long-period components could remain primarily assigned to hydrogen storage, while short-duration high-power peaks identified in the reconstructed signal could be partly managed by batteries for peak-shaving purposes. Similarly, the approach could be extended to other storage technologies, such as redox flow batteries, supercapacitors or thermal storage, according to their characteristic power, energy, efficiency and degradation behavior. Future work will focus on validating the spectral pre-sizing strategy against optimized time-domain solutions and on developing techno-economic criteria for flexible band allocation between storage technologies. In future work, the analysis will be extended to include a full validation of the methodology through comparison with optimized time-domain solutions, as well as a more detailed assessment of hybrid system performance.

Acknowledgements

This work was funded by the Community of Madrid through the R&D Activities Program in Technologies (2024), via the project SOLENER-CM, Ref. TEC-2024/ECO-31, under ORDER 5696/2024, dated December 10th (B.O.C.M. No. 307, pp. 108–129). This work was funded by the European Union's Horizon Europe research and innovation program under the POSEIDON project (POwer StoragE In D OceaN), Grant Agreement No. 101096457, funded under call HORIZON-CL5-2022-D5-01-02 – Innovative energy storage systems on-board vessels.

References

[1] Faisal M, Hannan MA, Ker PJ, Hussain A, Mansor M Bin, Blaabjerg F. Review of energy storage system technologies in microgrid applications: Issues and challenges. IEEE Access 2018;6:35143–64. https://doi.org/10.1109/ACCESS.2018.2841407.

[2] Wu D, Ma X. Modeling and Optimization Methods for Controlling and Sizing Grid-Connected Energy Storage: A Review. Current Sustainable/Renewable Energy Reports 2021 8:2 2021;8:123–30. https://doi.org/10.1007/s40518-021-00181-9.

[3] Zubiria A, Menéndez Á, Grande HJ, Meneses P, Fernández G. Multi-Criteria Decision-Making Problem for Energy Storage Technology Selection for Different Grid Applications. Energies 2022, Vol 15, 2022;15. https://doi.org/10.3390/en15207612.

[4] Alzahrani A, Ramu SK, Devarajan G, Vairavasundaram I, Vairavasundaram S. A Review on Hydrogen-Based Hybrid Microgrid System: Topologies for Hydrogen Energy Storage, Integration, and Energy Management with Solar and Wind Energy. Energies 2022, Vol 15, 2022;15. https://doi.org/10.3390/en15217979.

[5] Kotzur L, Markewitz P, Robinius M, Stolten D. Impact of different time series aggregation methods on optimal energy system design. Renew Energy 2018;117:474–87. https://doi.org/10.1016/j.renene.2017.10.017.

[6] Kotzur L, Markewitz P, Robinius M, Stolten D. Time series aggregation for energy system design: Modeling seasonal storage. Appl Energy 2018;213:123–35.

[7] Scott IJ, Carvalho PMS, Botterud A, Silva CA. Clustering representative days for power systems generation expansion planning: Capturing the effects of variable renewables and energy storage. Appl Energy 2019;253:113603.

[8] Yeganefar A, Amin-Naseri MR, Sheikh-El-Eslami MK. Improvement of representative days selection in power system planning by incorporating the extreme days of the net load to take account of the variability and intermittency of renewable resources. Appl Energy 2020;272:115224.

[9] Sánchez-Pérez PA, Staadecker M, Szinai J, Kurtz S, Hidalgo-Gonzalez P. Effect of modeled time horizon on quantifying the need for long-duration storage. Appl Energy 2022;317:119022.

[10] Oh E, Son S-Y. Energy-storage system sizing and operation strategies based on discrete Fourier transform for reliable wind-power generation. Renew Energy 2018;116:786–94.

[11] Cao Y, Wu Q, Zhang H, Li C. Optimal sizing of hybrid energy storage system considering power smoothing and transient frequency regulation. International Journal of Electrical Power & Energy Systems 2022;142:108227.

[12] Feng S, Wei W. Hybrid energy storage sizing in energy hubs: A continuous spectrum splitting approach. Energy 2024;300:131504. https://doi.org/https://doi.org/10.1016/j.energy.2024.131504.